A CYCLIC ELASTO-PLASTIC CONSTITUTIVE MODEL TO DESCRIBE DRAINED AND UNDRAINED TORSIONAL SHEAR BEHAVIOR OF SAND

Laddu Indika Nalin DE SILVA[1], Junichi KOSEKI[2] and Takeshi SATO[3]

ABSTRACT: A cyclic elasto-plastic constitutive model to describe the drained and undrained torsional shear behavior of sand is proposed. Stress-strain relationship under cyclic drained loading is modeled by incorporating a hyperbolic type stress-strain relationship with extended Masing's rules considering the damage to plastic shear modulus at large shear stress levels and hardening of the material with cyclic loading. Undrained cyclic shear behavior is modeled by assuming that the total volumetric strain increment during undrained loading, which consists of dilatancy and consolidation/swelling components, is equal to zero. Applicability of the proposed model is verified by simulating the results of a series of drained and undrained cyclic torsional shear tests on Toyoura sand. The stress-strain relationship, effective stress path and the liquefaction strength curve during cyclic loading are reasonably simulated by the proposed model.

Key Words: Hyperbolic stress-strain relationship, damage, hardening, stress-dilatancy relationship, liquefaction, cyclic torsional shear

INTRODUCTION

Soils are frequently subjected to large cyclic loadings due to traffic, sea waves and earthquakes. The type of loading condition can be drained, partially drained or undrained depending on the local soil conditions and frequency of loading. Among other issues associated with cyclic loading, liquefaction has been given a great deal of attention as the damage caused by liquefaction is disastrous and costly.

Therefore, researchers have been developing constitutive models based on various approaches to describe the behavior of soils under cyclic loading. One framework of cyclic elasto-plastic modelling to model the stress-strain relationship of soils under drained conditions is to model the monotonic loading curve (skeleton curve or backbone curve) by an appropriate type of function (usually hyperbolic) and apply the well known Masing's rule (Masing, 1926) with appropriate modifications to model the subsequent cyclic loading branches.

Tatsuoka et al. (2003) utilized the above approach successfully to simulate the stress-strain relationship of Toyoura sand subjected to cyclic plane strain compression under drained condition. Balakrishnaiyer (2000) employed a similar approach as above to successfully simulate the drained stress-strain relationship of Chiba gravel subjected to cyclic triaxial loading. The applicability of the above approach in simulating the stress-strain relationship of Toyoura sand subjected to drained cyclic torsional shear loadings was investigated by Hong Nam (2004).

[1] Post doctoral research fellow
[2] Professor
[3] Research support promotion member

However, it should be noted that all the models as described above are capable of reasonably simulating the stress-strain relationship of soils under drained condition well before its peak state (or less than 1 % of strain). In order to simulate large cyclic behavior with stress states closing its peak state, some modifications to the original concept may be necessary as the experimental evidences show damage to the soil structure at large stress levels causing reduction of plastic modulus of soil and hardening behavior of soil with subsequent cyclic loadings. In addition, there has been no attempt so far to the authors' knowledge to extend this approach to model the cyclic undrained behavior of soil.

In view of the above, it has been attempted in the present study to model the stress-strain relationship of sand subjected to large cyclic drained torsional shear loading by utilizing the same approach as proposed by Tatsuoka et al. (2003), while considering the damage to plastic properties at higher stress levels and hardening with subsequent cyclic loadings. The proposed model is employed to simulate the stress-strain relationship of Toyoura sand under drained cyclic torsional shear loading and it was combined with an empirical stress-dilatancy relationship to simulate the volumetric strain of sand under the same loading condition. Finally, a model is proposed to simulate the undrained cyclic torsional shear behavior of sand and hence liquefaction strength curve of Toyoura sand was obtained.

MODELLING OF DRAINED CYCLIC TORSIONAL SHEAR BEHAVIOR OF SAND

Modelling of skeleton curve

Hyperbolic type equations are widely employed to model non-linear stress-strain behavior of soil under drained condition. A typical hyperbolic equation has only two parameters with clear physical meanings namely, initial stiffness and peak strength, which can be determined in the laboratory. However, it was observed that the simulation using the above hyperbolic equation is not in good agreement with actual test data particularly at small strains (Tatsuoka and Shibuya, 1991a). Therefore, modified hyperbolic models have been proposed with more numbers of parameters. Tatsuoka and Shibuya (1991b) proposed a hyperbolic equation using parameters that are modeled as functions of strain to simulate stress-strain relations for wide range of strain. This equation is called as the Generalized Hyperbolic Equation (GHE) and takes the form as shown in Equation (1).

$$Y = \frac{X}{\dfrac{1}{C_1(X)} + \dfrac{|X|}{C_2(X)}} \tag{1}$$

in which, the normalized plastic shear strain and shear stress, $X = \gamma^p_{z\theta}/\gamma_{z\theta r}$ and $Y = \tau_{z\theta}/\tau_{z\theta max}$ are selected in the present study to model the torsional shear behavior of sand. $\gamma^p_{z\theta}$ is the plastic shear strain component, which was computed by subtracting the elastic shear strain component from total shear strain. Elastic shear strain component was evaluated by employing the recently developed IIS model (Hong Nam et al., 2005). $\gamma_{z\theta r}$ is the reference shear strain taken as the ratio of peak shear stress ($\tau_{z\theta max}$) and maximum quasi-elastic shear modulus ($G_{z\theta max}$). $\tau_{z\theta max}$ and $G_{z\theta max}$ of Toyoura sand of 75 % relative density at 100 kPa consolidation pressure was determined as 85 kPa and 100 MPa, respectively.

$C_1(X)$ and $C_2(X)$ are functions of strain, which can be determined by fitting to experimental data (refer to Hong Nam, 2004 for the details). Note that, $C_1(X = 0)$ represent the ratio of initial plastic shear moduli and initial quasi-elastic shear modulus, and $C_2(X = \infty)$ represent the normalized peak strength of the material.

Typical simulation of monotonic stress-strain relationship (skeleton curve) using the above equation along with the parameters used is shown in Fig. 1. It can be stated that the GHE can well simulate the skeleton curve of sand under torsional shear loading.

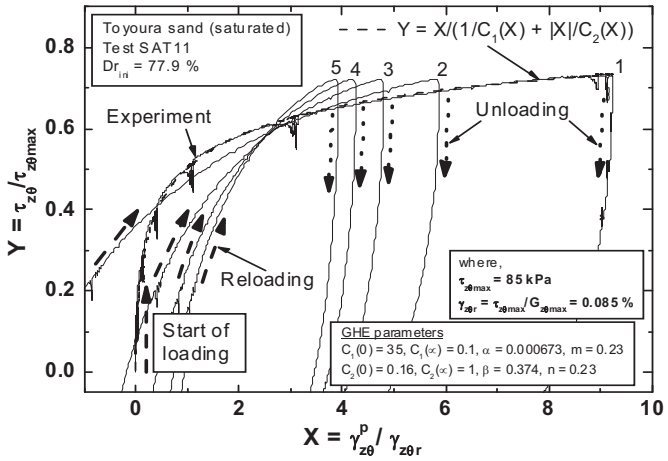

Figure 1. Modelling of skeleton curve of sand under torsional shear

Modelling of subsequent cyclic loading

Subsequent cyclic loading can be modeled by employing the extended Masing's rules (Tatsuoka et al, 2003). When the soil is subjected to cyclic loadings, rearrangement of particles takes place within the soil specimen. Tatsuoka et al. (2003) proposed a concept known as "drag" to take the particle rearrangement into account, in which the corresponding monotonic loading curve in opposite direction is dragged by an amount β when applying the Masing's rule during cyclic loading (extended Masing's rule). Refer to Fig. 2a for a schematic illustration of the concept of dragging and extended Masing's rule. Note that, the extended Masing's rule consists of several sub rules depending on the location of the current and previous turning points (refer to Tatsuoka et al., 2003 for the detailed explanation of these sub rules).

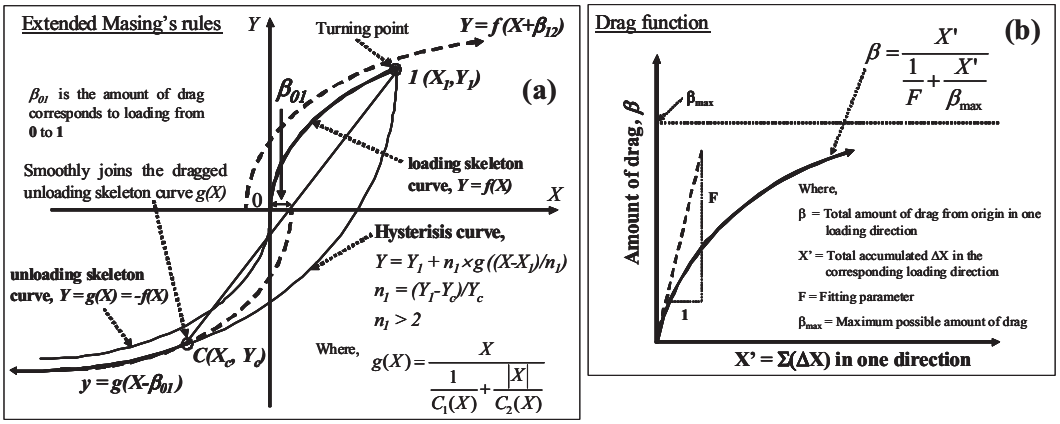

Figure 2. Application of extended Masing's rule in modeling the subsequent cyclic loadings

The amount of drag in a particular loading direction is assumed to be empirically related to the total accumulated normalized plastic shear strain, $X' = \Sigma(\Delta X)$, in the same direction up to the current turning point as schematically shown in Fig. 2b. Hong Nam (2004) suggested the values of the parameters F and β_{max} that are defined by the hyperbolic equation shown in Fig. 2b to be 0.45 and 3.13, respectively for cyclic torsional shear loading. The same values were employed in the current study.

Hardening and damage

Monotonic and cyclic stress-strain relationships of Toyoura sand specimens with similar densities under torsional shear loading are compared in Fig. 3. Although the peak strength values of the tests are similar to each other, effects of hardening due to the application of cyclic loading on the pre-peak behavior are evident.

Since the GHE tends to reach its asymptotic value near the peak stress state, the effects of drag in simulating the hardening behavior at higher stress levels is not significant; hence the simulation results start deviating from the experiment data when the stress state is closing its peak.

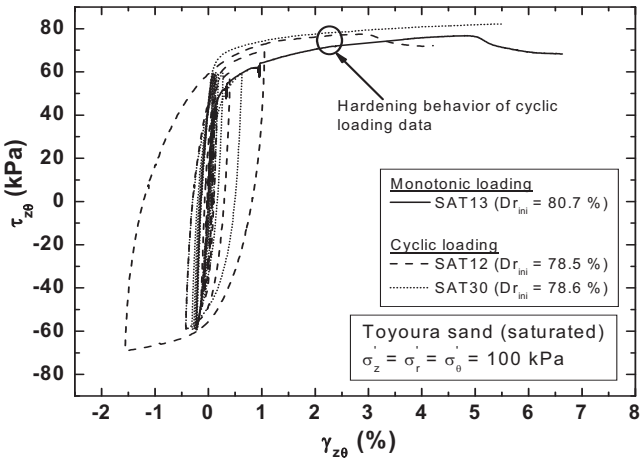

Figure 3. Hardening due to cyclic loading

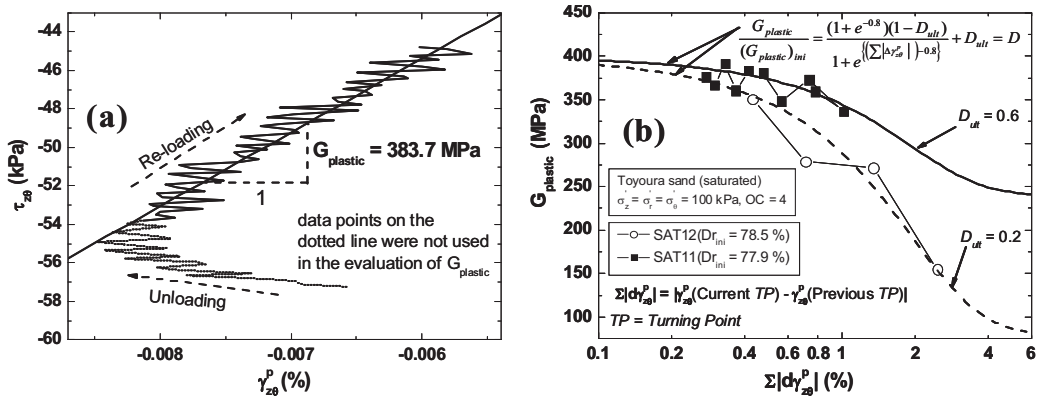

Figure 4. Damage to plastic shear modulus during large amplitude cyclic loading

In addition to the hardening due to cyclic loading, the soil fabric will undergo damage when subjected to higher shear stress levels. In order to further investigate the damage, plastic shear modulus ($G_{plastic}$) values at each turning point during cyclic loading were evaluated as typically shown in Fig. 4a. Note that the plastic shear modulus values were evaluated by linearly fitting to the linear portion of the shear stress versus plastic shear strain relationship when the specimen starts showing the plastic deformation at each turning point. These plastic shear moduli values were plotted against the accumulated $\gamma^p{}_{z\theta}$ between the current and previous turning points ($\Sigma| d\gamma^p{}_{z\theta}|$) as shown in Fig. 4b. Results show good correlation between $G_{plastic}$ and $\Sigma| d\gamma^p{}_{z\theta}|$ showing possible damage to soil fabric.

In the method proposed by Tatsuoka et al. (2003), a unique skeleton curve for a particular loading

direction was used when modeling the hysteresis curves using the extended Masing's rules. In order to consider in addition the effects of above hardening and damage in such modeling, the use of non-unique skeletons curves when applying the extended Masing's rule is proposed in the current study.

Hardening behavior with cyclic loading is taken into account by multiplying $C_2(X)$ of Eq. (1) by a hardening factor "S" (refer to Eq. (2)). The hardening factor "S" is assumed to be a function of the total normalized plastic shear strain that has been accumulated up to the current turning point, $\Sigma|\Delta X|$.

$$S = 1 + \frac{\left(\sum |\Delta X|\right)_{\text{Upto current turing point}}}{\frac{\beta_{\max}}{F} + \frac{\left(\sum |\Delta X|\right)_{\text{Upto current turing point}}}{(S_{ult} - 1)}} \tag{2}$$

where, S_{ult} = the highest value for S (taken as 1.35 and 1.15 for constant stress amplitude cyclic loading and varying stress amplitude cyclic loadings, respectively). When hardening and damage are considered in the model, the drag parameters F and β_{max} are modified into 0.15 and 12.0, respectively. These parameters were determined by trial and error. It should be emphasized that more experimental investigations on this issue is required for better understanding of the phenomenon.

Damage to the plastic shear moduli is taken into account by multiplying $C_1(X)$ of Eq. (1) by a damage factor "D" (refer to Eq. (3)). Experimental evidences as shown in Fig. 4 suggest that the damage factor "D" can be taken as a function of the accumulated plastic shear strain between the current and previous turning points ($\Sigma|d\gamma^p_{z\theta}|$).

$$D = \frac{(1 + e^{-0.8})(1 - D_{ult})}{1 + e^{\left\{\left(\sum \left|d\gamma^p_{z\theta}\right|\right) - 0.8\right\}}} + D_{ult} \tag{3}$$

where, D_{ult} = the ratio of plastic shear modulus at peak shear strain and the initial plastic shear modulus (D_{ult} is taken as 0.2). Note that the initial plastic shear modulus was evaluated by linearly fitting to the initial linear portion of the shear stress versus plastic shear strain relationship when the specimen starts showing the plastic deformation. It is assumed that D = 1 (no damage) until the stress state first exceeds the phase transformation stress state at which volumetric behavior changes from contractive to dilative, as will be explained later in details. Note that factors "S" and "D" are constants for a particular loading branch but varies with different branches.

STRESS-DILATANCY RELATIONSHIP

Modeling of stress-strain relationship as discussed above is not sufficient to describe the volumetric behavior of soil. Therefore, a relationship that deals with the ratio of plastic volumetric and shear strain increments to a shear stress ratio is required in addition to the stress-strain relationship. This relationship is known as the stress-dilatancy relationship.

There are various theoretical stress-dilatancy relationships available for triaxial and plane strain loading conditions. It should be noted that all those stress-dialtancy relations are originally developed for monotonic loading conditions. Pradhan and Tatsuoka (1989) experimentally investigated the stress-dilatancy relationships of sand subjected to cyclic loading conditions and modified the available stress-dilatancy relationships to apply for cyclic loading conditions.

However, it should be noted that the theoretical stress-dilatancy relations were derived mostly for either cyclic triaxial ($d\varepsilon_2 = d\varepsilon_3$) or cyclic plane strain (or simple shear) ($d\varepsilon_2 = 0$) loading conditions. Therefore, in order to deal with more general deformation mode such as torsional shear, an empirical

stress-dilatancy relationship is employed in the present study.

As shown in Fig. 5, results from cyclic torsional shear experiment suggest that unique relationships between the shear stress ratio ($\tau_{z\theta}/p'$) and the dilatancy ratio ($-d\varepsilon^p_{vol}/d\gamma^p_{z\theta}$) exist for $d\gamma^p_{z\theta} > 0$ and $d\gamma^p_{z\theta} < 0$, respectively. Higher dilatancy ratios can be observed immediately after the reversal of loading direction. In addition, the effects of over-consolidation alter the stress-dilatancy relationship during virgin loading as shown in Fig. 5b. Therefore, the following bilinear equation can be proposed by referring to the experiment data as shown in Fig. 5 to model the stress-dilatancy relationship during subsequent cyclic loadings.

$$\frac{\tau_{z\theta}}{p'} = R_k\left(-\frac{d\varepsilon^p_{vol}}{d\gamma^p_{z\theta}}\right) + C \tag{4}$$

where, the average value of R_k is taken as 1.5 and the average value of C is taken as 0.46 and -0.46 for $d\gamma^p_{z\theta} > 0$ and $d\gamma^p_{z\theta} < 0$, respectively. In order to consider the stress-dilatancy relationships immediately after the reversal of loading direction, R_k is taken as 0.33 and C is taken as -0.18 and 0.18 for $d\gamma^p_{z\theta} > 0$ and $d\gamma^p_{z\theta} < 0$, respectively (refer to Fig. 5a and 5b).

Stress-dilatancy relationship of normally consolidated Toyoura sand during virgin loading (refer to Fig. 5a) is modeled separately (Nishimura, 2002) by taking R_k as 1.3 and C as 0.60, while that of over-conslidated Toyoura sand (refer to Fig. 5b) will be discussed later.

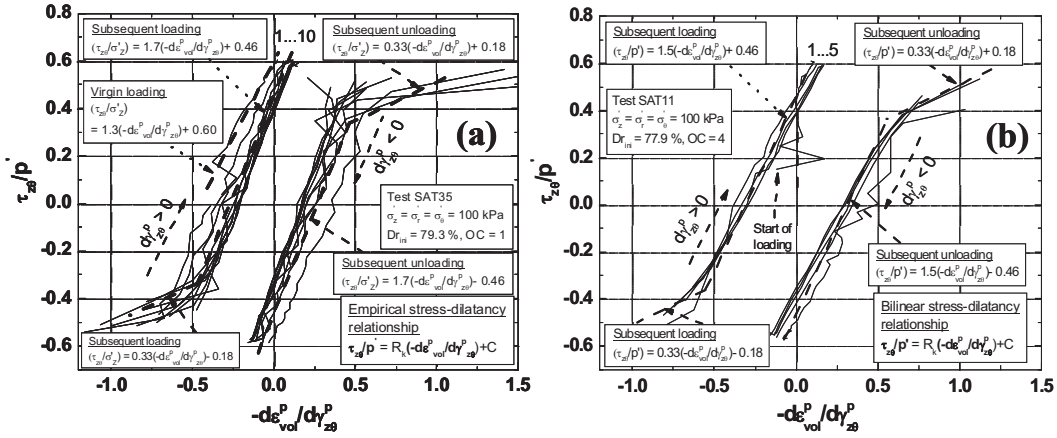

Figure 5. Bilinear stress-dilatancy relationship

Effects of hardening and damage on stress-dilatancy relationship

It can be seen in Fig. 5 that the effects of hardening and damage cause slight variations in the stress-dilatancy relationship during subsequent cyclic loadings. Note that the $|C|$ values during constant stress amplitude cyclic torsional loading becomes smaller with subsequent cyclic loadings as shown in Fig. 5a and 5b (1..10 in Fig. 5a corresponds to the cyclic number). Furthermore, the $|C|$ value can even become larger, depending on the accumulated strain during the previous reloading/re-unloading branch.

Considering the above factors, the bilinear stress-dilatancy model as proposed before was further modified as shown below by introducing the damage factor D.

$$\frac{\tau_{z\theta}}{p'} = (R_{\max} \times D\ ) \times \left(-\frac{d\varepsilon^p_{vol}}{d\gamma^p_{z\theta}}\right) + \frac{C_{\min}}{D} \tag{5}$$

where, R_{max} = the maximum value of R_k in Eq. 4 (R_{max} = 1.5 was selected). C_{min} = the minimum value of C (C_{min} = $\pm$0.36 was assumed for $d\gamma^p_{z\theta} > 0$ and $d\gamma^p_{z\theta} < 0$, respectively). Two boundary conditions were specified for $R_{max}\times D$ value and $|C_{min}/D|$ value by referring to the experimental data. If $R_{max}\times D$ value becomes less than 1.00, $R_{max}\times D$ = 1.00 was used. If $|C_{min}/D|$ becomes greater than 0.50, $|C_{min}/D|$ = 0.50 was used.

Therefore, $R_{max}\times D$ value in Eq. 5 varies between 1.5 and 1.0, and $|C_{min}/D|$ value varies between 0.36 and 0.50 depending on the accumulated strain between current and previous turning points (i.e. damage parameter, D). Note that the above modification was applied only to the main body of the bilinear stress-dilatancy relationship. The stress-dilatancy relationships immediately after the stress-reversal as shown in Fig. 5 was not modified (i.e. R_k = 0.33 and C = $\pm$0.18 for $d\gamma^p_{z\theta} > 0$ and $d\gamma^p_{z\theta} < 0$, respectively). Furthermore, the stress-dilatancy relationship during virgin loading was also not modified.

The value of $d\gamma^p_{z\theta}$ in Eq. 5 can be obtained from the simulation of stress-strain relationship. Then, ε^p_{vol} can be evaluated by numerically integrating $d\varepsilon^p_{vol}$ in Eq. 5.

MODELLING OF UNDRAINED CYCLIC TORSIONAL SHEAR BEHAVIOR

One framework for modeling the undrained torsional shear behavior of soil is to assume that the total volumetric strain increment $(d\varepsilon_{vol})$ during undrained loading, which is equal to zero, consists of a volumetric strain component purely due to shear stress (or dilatancy, $d\varepsilon^d_{vol}$) and a volumetric strain component purely due to consolidation/swelling of the soil ($d\varepsilon^c_{vol}$) due to the change in mean effective stress (p'). Hence the following equation is assumed to be valid during the cyclic undrained loading.

$$d\varepsilon^c_{vol} + d\varepsilon^d_{vol} = 0 \tag{6}$$

$d\varepsilon^d_{vol}$ can be evaluated by combining the modeling of stress-strain relationship during cyclic drained loading with the stress-dilatancy relationship. It is assumed that there exists a unique relationship between $(\tau_{z\theta}/p')/(\tau_{z\theta}/p')_{max}$ and $\gamma^p_{z\theta}/\gamma_{z\theta r}$ (where, $\gamma_{z\theta r} = (\tau_{z\theta}/p')_{max}/(G_{z\theta max}/p'_o)$) among drained and undrained loadings (note that p' is kept constant, hence $p' = p'_o$ in drained tests), hence the same stress-dilatancy relationship as proposed in Eq. 5 can be employed to evaluate $d\varepsilon^d_{vol}$ during undrained loading.

However, accurate determination of $(\tau_{z\theta}/p')_{max}$ of dense sand subjected to drained and undrained torsional shear loadings is a difficult task in the current study because the capacity of shear strain measurement employed is limited to about 5 % of single amplitude shear strain. Therefore, GHE parameters for undrained loading are determined by slightly modifying the drained parameters for better simulation of the undrained behavior.

Effects of over-consolidation on stress-dilatancy relationship

It is evident from Fig. 5b that the effects of over-consolidation significantly affect the stress-dilatancy relationship during virgin loading and its effects vanish with subsequent cyclic loadings. Note that p' is kept constant during drained cyclic torsional shear tests in the current study. However, during cyclic undrained loading, the specimen is continuously subjected to over-consolidation, which may have significant effects on the stress-dilatancy relationship, which is proposed in Eq. 5.

During undrained cyclic loading, firstly, the soil is subjected to over-consolidation until the stress state exceeds the phase transformation stress state for the first time (i.e. the first instance where the volumetric behavior changes from contractive to dilative ($dp' > 0$). Phase transformation stress state for virgin loading is taken as $|\tau_{z\theta}/p'| = C = 0.60$, and for subsequent cyclic loadings, it is determined as $|\tau_{z\theta}/p'| = C = 0.50$). Note that, in Eq. 4, the average value of C is taken as 0.46, while C = 0.50 corresponds to the maximum value of C during subsequent cyclic loading (i.e. the boundary value of

$|C_{min}/D|$ in Eq. 5). Then the soil will enter the stage of cyclic mobility. The stress-dilatancy relationships during these two stages will be addressed separately in the current study.

After the stress state enters the cyclic mobility for the first time, the stress-dilatancy relationship during cyclic torsional loading can be modeled by the modified bilinear stress-dilatancy relationship as expressed in Eq. 5. Before the stress state exceeds the phase transformation stress state for the first time (before cyclic mobility), the effects of over-consolidation need to be taken into account for better simulation of the cyclic undrained behavior. Oka et al. (1999) proposed a stress-dilatancy equation to consider the effects of over-consolidation. A similar equation was employed in the current study as shown in Eq. 7.

$$\left(-\frac{d\varepsilon_{vol}^{p}}{d\gamma_{z\theta}^{p}}\right)=D_k\left(\frac{\tau_{z\theta}}{p'}-\left(\frac{\tau_{z\theta}}{p'}\Big/\ln(OC)\right)\right)\Big/\left(R_s\right) \tag{7}$$

where, $D_k=\left[\left|\tau_{z\theta}/p'\right|/(C_s\times\ln(OC))\right]^{1.5}$, OC = over-consolidation ratio, R_s and C_s are taken as 2.2 and 0.50, respectively.

Eq. 7 is employed when D_k is less than or equal to 1.0 during cyclic undrained loading until the stress state first exceeds the phase thansformation stress state. When D_k = 1, Eq. 7 becomes identical to Eq. 4 with R_k and C being replaced by R_s and C_s, and follows the stress dilatancy relationship given by Eq. 4 afterwards. Therefore D_k = 1 denotes the over-consolidation boundary surface.

The above equation was used in the drained tests as well, if the specimen is subjected to over-consolidation.

Evaluation of $d\varepsilon^{e}_{vol}$

Experimental evidences as shown in Fig. 6a suggests that the quasi-elastic bulk moduli ($K = dp'/d\varepsilon^{e}_{vol}$) can be expressed as a function of p' for a given density as shown in Eq. 8 (note that the effect of the change in void ratio during consolidation from p' = 100 kPa to 400 kPa on the K value is considered implicitly in the equation, i.e. $f(e) = f(e_o)$).

$$\frac{K}{f(e)}=\frac{K_o}{f(e_o)}\left(\frac{p'}{p'_o}\right)^{m_k} \tag{8}$$

where, K_o is the bulk modulus at a reference stress state p'_o and m_K is the parameter to express the stress state dependency of K. According to the experiment data as shown in Fig. 6a, K_o at p'_o = 100 kPa is obtained as 80 MPa for a Toyoura sand specimen of about 75 % relative density. The average value of m_k is 0.643. Note that, the K_o values for other densities as shown in Fig. 6a were evaluated by assuming that the K_o values normalized by the void ratio function $f(e_o)$(Hardin and Richart, 1963) at the same reference stress state are unique among different densities.

Since it is believed that the swelling behavior of sand is nearly elastic, the total volumetric strain due to swelling (ε^{e}_{vol}) is evaluated by integrating its increment ($d\varepsilon^{e}_{vol}$) given by Eq. 8, and compared with the corresponding experiment data as shown in Fig. 6b. However, it can be observed from Fig. 6b that the specimen exhibits generation of some plastic volumetric strain even during swelling.

Therefore, in order to take the generation of plastic volumetric strain into account, K_o at p'_o = 100 kPa is taken as 58 MPa for a Toyoura sand specimen of about 75 % relative density and the value of m_k is taken as 0.9. It can be observed that ε^{e}_{vol} evaluated by applying the above parameters in Eq. 8 reasonably matched with the experiment data as shown in Fig. 6b.

Then, by combining Eqs. 6 and 8, we can get the following relationship between dp' and $d\varepsilon^{d}_{vol}$.

$$dp'=K_o\left(p'/p'_o\right)^{m_k}\times(-d\varepsilon^{d}_{vol}) \tag{9}$$

Therefore, the stress path and stress-strain relationship of sand subjected to undrained cyclic torsional shear loading can be modeled by employing Eq. 9.

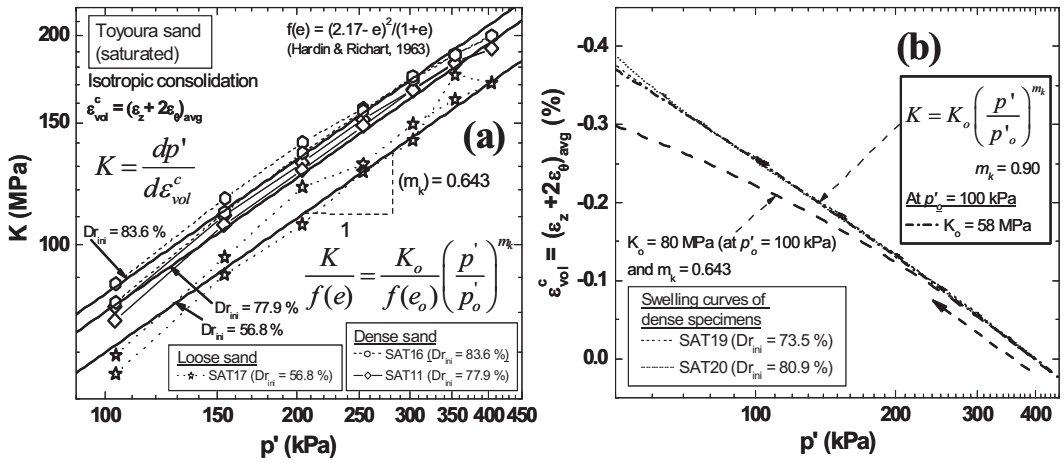

Figure 6. Modelling of the swelling behavior of sand

SIMULATION OF TEST RESULTS AND DISCUSSION

Simulation of cyclic drained behavior of sand

Simulations results of stress-strain relationships of sand subjected to drained cyclic torsional shear loading are shown in Figs. 7, 8 and 9. In order to illustrate the improvement achieved, first the simulation was carried out by employing the original Masing's rule (Case 1) (without the drag) as shown in Fig. 7. It can be seen in Fig. 7a that the original Masing's rule is not capable of simulating the constant stress amplitude cyclic loading and ended up tracing an identical curve for subsequent cyclic loadings, while experimental data shows hardening behavior with the subsequent cyclic loading. In addition, the simulation results of varying stress amplitude cyclic loading start deviating from the experiment data when the stress states become closer to the peak strength as shown in Fig. 7b.

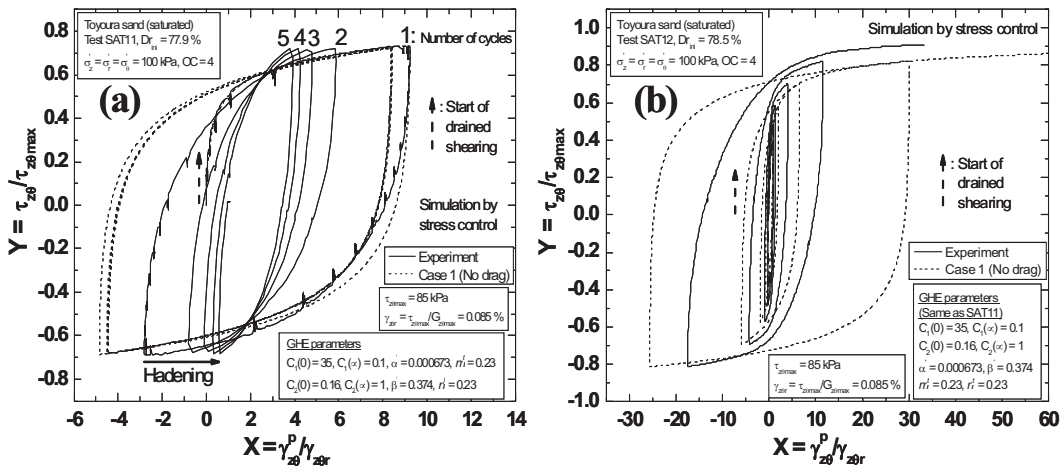

Figure 7. Simulation of stress-strain relationship using the original Masing's rule

Then the concept of drag is introduced into the simulation as shown in Fig. 8 (Case 2). It can be seen that, except for the first cycle, no significant improvement can be observed in the simulation of constant stress amplitude cyclic loading as shown in Fig. 8a. On the other hand, simulation is improved up to a certain extent in case of varying stress amplitude cyclic loading as shown in Fig. 8b. However, the simulation results start deviating from the experiment data when the stress state is closing its peak.

Finally, simulation is further modified by introducing the hardening and damage into the model as shown in Fig. 9 (Case 3). It can be seen that the simulation results of constant and varying stress amplitude cyclic loadings (Fig. 9a and Fig. 9b, respectively) are reasonably consistent with the experiment data after introducing hardening and damage to the extended Masing's rules.

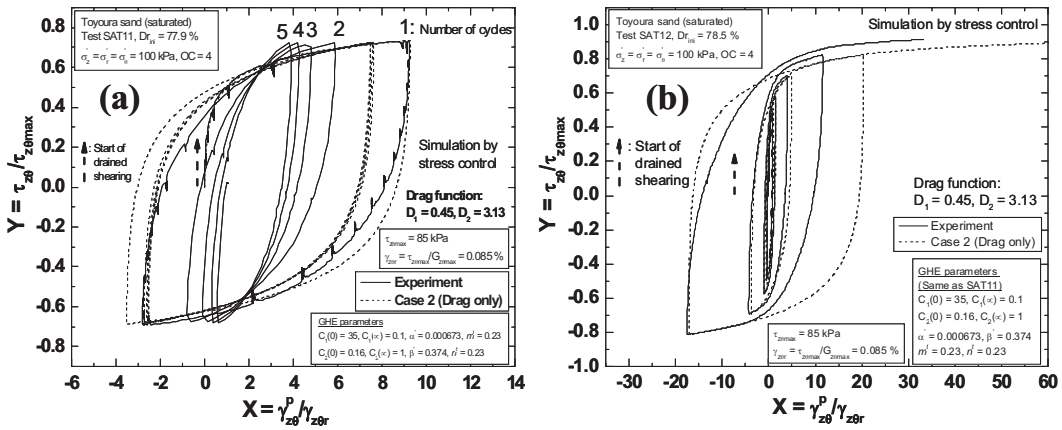

Figure 8. Simulation of stress-strain relationship using the Extended Masing's rule

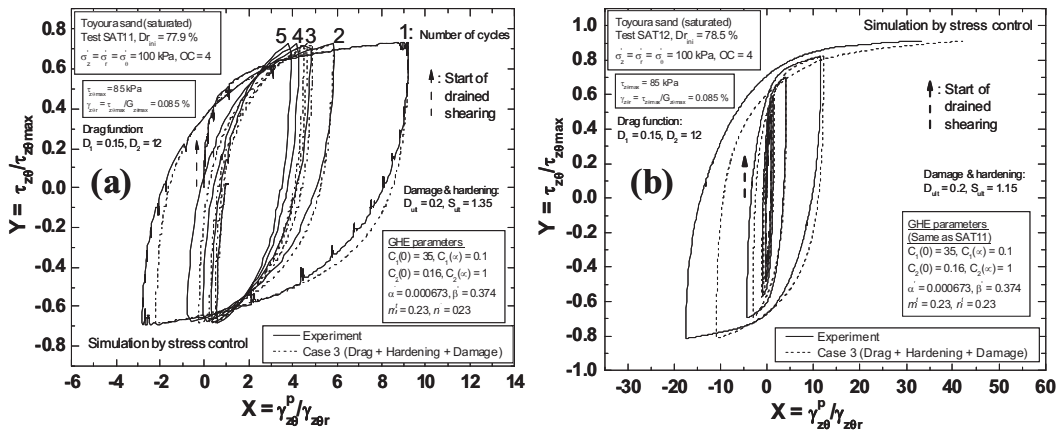

Figure 9. Simulation of stress-strain relationship with hardening and damage

Simulation of volumetric behavior of sand

Simulation of ε^p_{vol} during drained cyclic torsional shear loading was carried out, first by employing the bilinear stress-dilatancy relationship (Eq. 4)(denoted as Case A), and then by employing the modified bilinear stress-dilatancy relationship (Eq. 5)(Case B) in order to illustrate the improvement achieved. $d\gamma^p_{z\theta}$ values in Eqs. 4 and 5 were computed by using the Case 3 stress-strain simulation since it is reasonably consistent with the experiment data.

Comparison of simulation of ε^p_{vol} with corresponding experiment data of two typical experiments are shown in Fig. 10a and Fig. 10b. It is evident that hardening of the material due to constant stress amplitude cyclic torsional loading causes reduction of the accumulation of ε^p_{vol} with subsequent cyclic loadings as shown in Fig. 10a. However, simulation of ε^p_{vol} by using bilinear stress-dilatancy model (Case A of Fig. 10a) do not well conform with the experiment data showing nearly constant accumulation of ε^p_{vol} with subsequent cyclic loadings.

In addition, the large accumulation of ε^p_{vol} immediately after the reversal of loading direction at large shear stress levels as shown in Fig. 10b can not be well simulated by employing the bilinear stress-dilatancy model (Case A of Fig. 10b).

On the other hand, It can be observed that the simulation is significantly improved when the slight variations in stress-dilatancy relationship due to hardening and damage is taken into account by employing the modified bilinear stress-dilatancy model as shown in Case B of Fig. 10a and Fig. 10b.

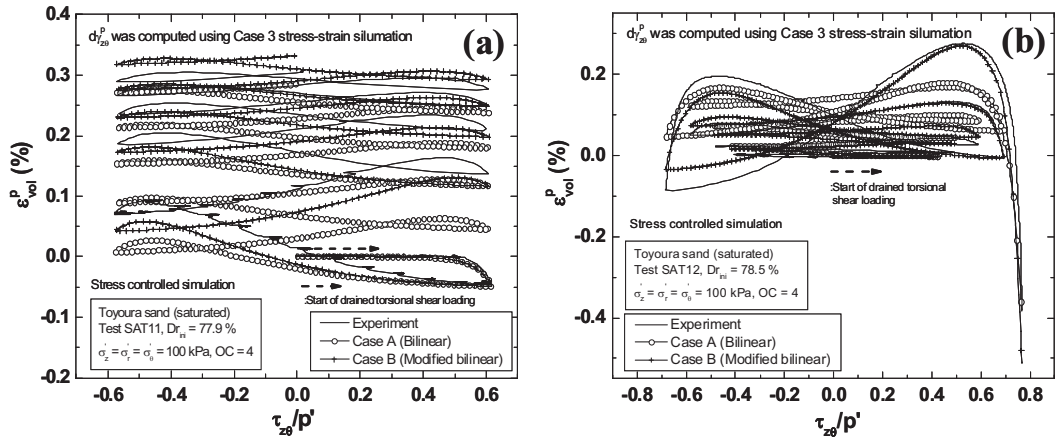

Figure 10. Simulation of volumetric strain

Simulation of liquefaction behavior of sand

Fig. 11 shows the comparison of experimentally obtained stress paths and stress-strain relationships of a typical undrained cyclic torsional shear test (refer to Fig. 11a and Fig. 11b, respectively) and its simulation (Note that, the elastic strain component can be neglected compared to the total shear strain, hence $\gamma_{z\theta} \approx \gamma^p_{z\theta}$ is assumed in the comparison of experiment data with its simulation).

First, the simulation of stress path and stress-strain relationship was carried out by employing the modified bilinear stress-dilatancy relationship to evaluate $d\varepsilon^d_{vol}$ as shown in Fig. 11c and Fig. 11d. The effect of change of over-consolidation ratio on stress-dilatancy relationship was not considered in the above simulation.

Then the effect of over-consolidation on the stress-dilatancy relationship was taken into account in the simulation by employing Eq. 7 within the over-consolidation boundary surface ($\tau_{z\theta} < \pm p' \times C_s \times ln(OC)$) as shown in Fig. 11e and Fig. 11f.

It is clear from Fig. 11e and Fig. 11f that the simulation of both stress path and stress-strain relationship is improved after introducing the effects of over-consolidation on stress-dilatancy relationship in the simulation.

However, experimentally obtained stress-strain relationship of dense Toyoura sand (refer to Fig. 11b) shows continuous and more regular increase in the shear strain amplitude even after the stress path enters the steady state of cyclic mobility, while simulation results show reasonable agreement with the experiment data until the stress path enters the steady state, and ended up tracing a closed loop after the stress path enters the steady state. Further modifications that might consider the strain

softening behavior of sand would be required in the simulation to address the above issue, which is out of the scope of the current study.

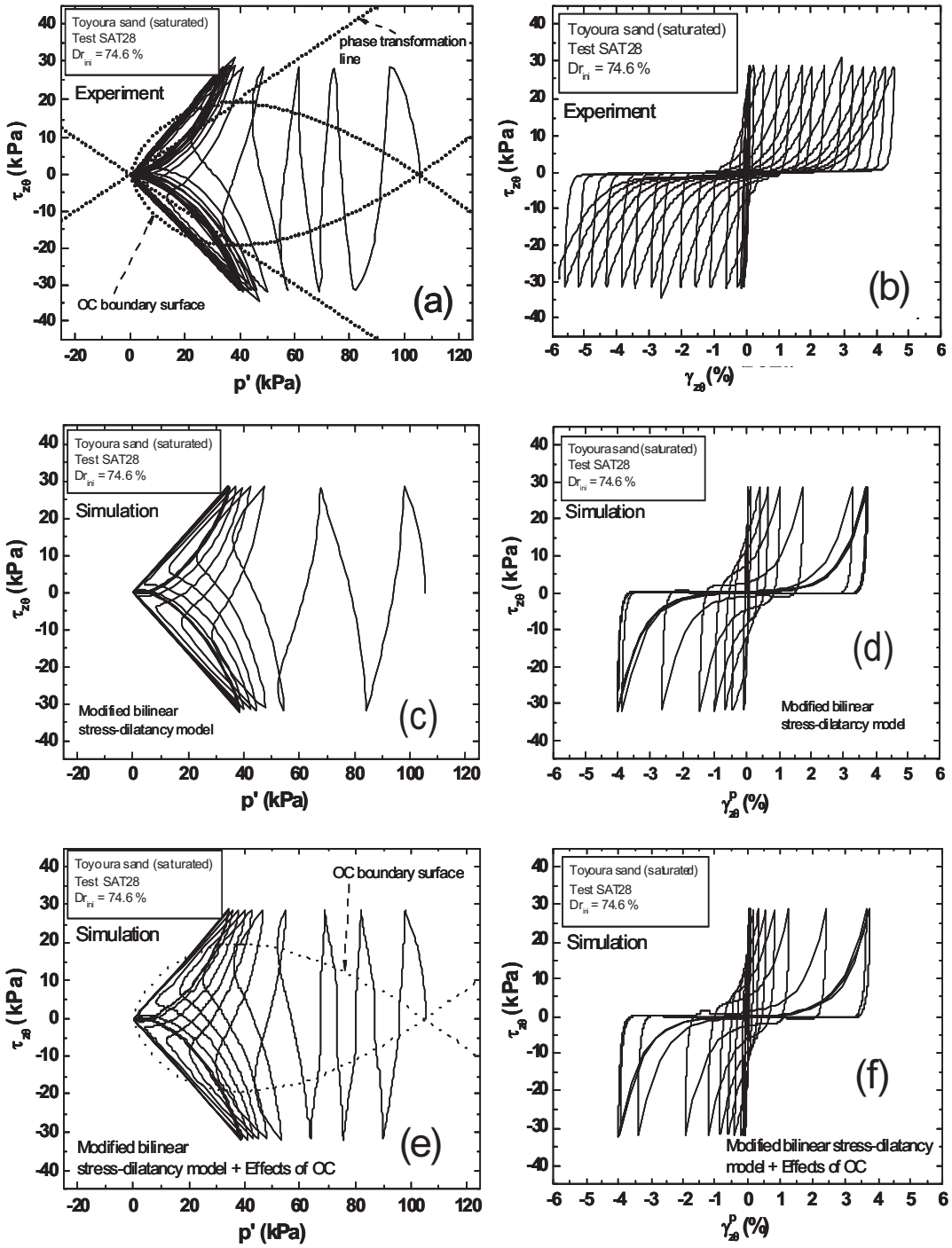

Figure 11. Simulation of the liquefaction behavior of sand

Fig. 12 shows the liquefaction resistance curves of dense Toyoura sand obtained from the experimental and simulation results. Liquefaction resistance is defined as the number of cycles required to induce a double amplitude shear strain (DA) of 6 %. It can be seen that simulation could be significantly improved when the modified bilinear stress-dilatancy relationship was employed in the simulation, while considering the effects of over-consolidation.

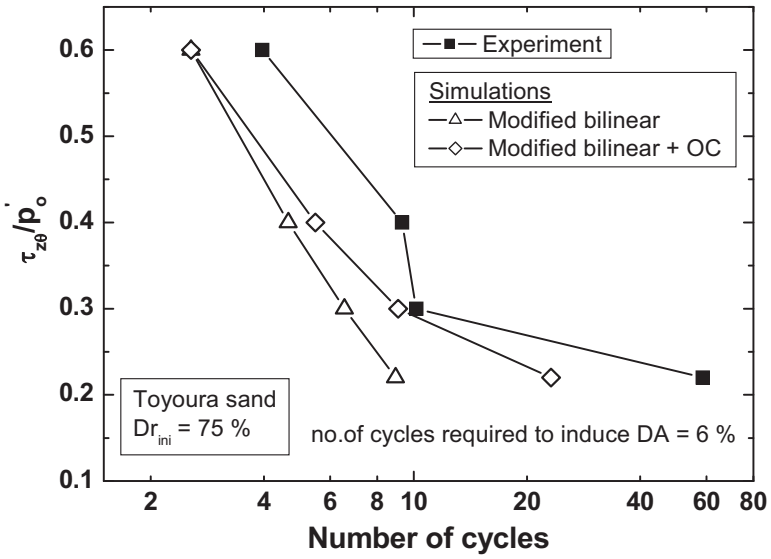

Figure 12. Liquefaction resistance curve

CONCLUSIONS

A cyclic elasto-plastic constitutive model based on a hyperbolic type stress-strain relationship, extended Masing's rules and an empirical stress-dilatancy relationship is proposed to simulate the drained and undrained cyclic torsional shear behavior of sand. The main findings of the current study could be summarized as follows.

a) Stress-strain relationship of Toyoura sand subjected to drained cyclic torsional shear loading could be reasonably simulated by the proposed model after considering the hardening behavior due to cyclic loading, and damage to plastic shear modulus at higher shear stress levels.
b) An empirical bilinear stress-dilatancy relationship that varies with the amount of damage to the plastic shear modulus of the material is proposed. Accumulation of plastic volumetric strain due to the application of drained cyclic torsional shear loading could be reasonably simulated by the proposed stress-dilatancy relationship.
c) The proposed model is capable of reasonably simulating the liquefaction behavior of dense sand until the specimen enters the steady state. Liquefaction resistance of dense Toyoura sand could be reasonably reproduced by the proposed model.

REFERENCES

Balakrishnayer, K. (2000). "Modelling of deformation characteristics of gravel subjected to large cyclic loading." *Ph.D. thesis*, Department of civil engineering, The University of Tokyo, Japan.

Hardin, B. O. and Richart, F. E., Jr. (1963). "Elastic wave velocities in granular soils." *Journal of soil mechanics and foundation division*, Vol. 89, No. 1, ASCE, 33-65.

Hong Nam, N. and Koseki, J. (2005). “Quasi-elastic deformation properties of toyoura sand in cyclic triaxial and torsional loadings.” *Soils and Foundations*, Vol. 45, No. 5, 19-38.

HongNam, N. (2004). “Locally measured quasi-elastic properties of toyoura sand in cyclic triaxial and torsional loadings and their modeling.” *PhD thesis*, Dept. of Civil Engineering, The University of Tokyo, Japan.

Masing, G. (1926). “Eiganspannungen und verfestigung beim messing.” *Proceedings of the Second International Conference of Applied Mechanics*, 332-335.

Nishimura, S. (2002). “Development of three dimensional stress-strain model of sand undergoing cyclic undrained loading and stress-axes rotation.” *M.Eng thesis*, Dept. of Civil Engineering, The University of Tokyo, Japan.

Oka, F., Yashima, A., Tateishi, Y., Taguchi, Y. and Yamashita, S. (1999). “A cyclic elasto-plastic constitutive model for sand considering a plastic-strain dependence of the shear modulus.” *Geotechnique*, Vol. 49, No. 5, 661-680.

Pradhan, T.B.S. and Tatsuoka, F (1989). “On stress-dilatancy equations of sand subjected to cyclic loading.” *Soils and Foundations*, Vol.29, No.1, 65-81.

Tatsuoka, F. and Shibuya, S. (1991a). “Modelling of non-linear stress-strain relations of soils and rocks- Part 1: Discussion of hyperbolic equation.” *Seisan-kenkyu, Journal of IIS*, The University of Tokyo, Vol. 43, No. 9, 409-412.

Tatsuoka, F. and Shibuya, S. (1991b). “Modelling of non-linear stress-strain relations of soils and rocks- Part 2: New Equation.” *Seisan-kenkyu, Journal of IIS*, The University of Tokyo, Vol. 43, No. 10, 435-437.

Tatsuoka, F., Masuda, T., Siddiquee, M. S. A. and Koseki, J. (2003). “Modeling the stress-strain relations of sand in cyclic plane strain loading.” *Journal of Geotechnical and Geoenvironmental Engineering*, Vol. 129, No. 6, ASCE, 450-467.